



# Peroxidase activity of new mixed-valence cobalt complexes with ligands derived from pyridoxal

Liniquer André Fontana<sup>1</sup> | Josiéli Demetrio Siqueira<sup>1</sup> | Joice Ceolin<sup>1</sup> |Bernardo Almeida Iglesias<sup>2</sup> | Paulo Cesar Piquini<sup>3</sup> | Ademir Neves<sup>4</sup> | Davi Fernando Back<sup>1</sup>

<sup>1</sup>Laboratório de Materiais Inorgânicos – Departamento de Química, CCNE, UFSM, 97105-900 Santa Maria, RS, Brazil

<sup>2</sup>Laboratório de Bioinorgânica e Materiais Porfirínicos, CCNE, UFSM, 97105-900 Santa Maria, RS, Brazil

<sup>3</sup>Departamento de Física, CCNE, UFSM, 97105-900 Santa Maria, RS, Brazil

<sup>4</sup>Departamento de Química, Universidade Federal de Santa Catarina, UFSC, 88040-970 Florianópolis, SC, Brazil

## Correspondence

Davi Fernando Back, Laboratório de Materiais Inorgânicos – Departamento de Química, CCNE, UFSM, 97105-900, Santa Maria, RS, Brazil.

Email: davi.f.back@ufsm.br

## Funding information

Brazilian Research Councils: CNPq, Grant/Award Number: Proc. Num. 444780/2014-9, 303011/2016-5 and 424514; UFSM/CNPQ-PIBIC, Grant/Award Number: 2016 (043272); FAPERGS, Grant/Award Number: ED. 02/2017 - PqG; UFSM/CNPQ-PIBIC-2016, Grant/Award Number: 443625-2014-0

New mixed-valence cobalt complexes with ligands derived from pyridoxal were synthesized and characterized, and their application as mimetics of the peroxidase enzyme was investigated. Single-crystal X-ray diffraction was used to analyze all complex structures in the solid state and their electrochemical behavior was investigated. A reactivity pattern was observed in the complex synthesis regarding the cobalt compounds from which analogous zwitterionic derivatives were obtained. The importance of these compounds lies in understanding their behavior in an oxidizing environment and evaluating whether they can activate hydrogen peroxide to oxidize phenolic compounds. In nature, enzymes called peroxidases, which efficiently oxidize phenolic compounds, trigger many reactions involving the activation of hydrogen peroxide to oxidize organic substrates. However, these enzymes present several disadvantages, including denaturation and elevated costs. Therefore, these limitations can be overcome by expanding research into the study of synthetic catalysts for the oxidation of phenolic compounds using hydrogen peroxide, which is a highly relevant field of bioinorganic chemistry.

## KEYWORDS

cobalt, peroxidase activity, pyridoxal, zwitterionic complexes

## 1 | INTRODUCTION

New polydentate ligands associated with N, O, and S atoms have been attracting increasing interest in coordination chemistry and associated areas (mainly bioinorganic chemistry, catalysis, and material science).<sup>[1–3]</sup> In bioinorganic chemistry, coordination complexes with these ligands are widely studied as enzymatic mimetics.<sup>[4–6]</sup> This is because the active sites of many metalloenzymes exhibit nitrogen and sulfur (nitrile hydratase),<sup>[7]</sup> nitrogen and oxygen (SOD-Mn),<sup>[8]</sup> or even

combinations of N, S, and O atoms (alcohol dehydrogenase),<sup>[9]</sup> which form the coordination sphere of the metal.

Therefore, the present study aimed to explore ONS Schiff base-type ligands with nitrogen derived from an azomethine group (imine), oxygen from a phenol group, and sulfur from a thioether group. Schiff bases are versatile ligands in coordination chemistry<sup>[10]</sup> that are easily obtained by the reaction between a primary amine and an aldehyde.

Pyridoxal was chosen for ligand synthesis due to its rich coordination chemistry.<sup>[11]</sup> This aldehyde is a

derivative of vitamin B6 and the cofactor of several enzymatic reactions related to protein metabolism, especially transamination, racemization, and decarboxylation of amino acids.<sup>[11,12]</sup> Therefore, Schiff base-type ligands were obtained from the reaction of pyridoxal with 2-aminothiophenol derivatives.

Cobalt complexes with Schiff bases, which can reversibly bind to oxygen and carbon dioxide,<sup>[13]</sup> are a new alternative for the catalytic activation of these substances. In addition, they are efficient catalysts for the oxidation of olefins and oxidative coupling of phenols<sup>[14]</sup> and aromatic amines.<sup>[15–17]</sup> Therefore, the main interest in the compounds synthesized in this study is their behavior in the oxidizing environment and whether hydrogen peroxide can be activated through the oxidation of phenolic compounds and aromatic amines. In nature, many reactions involving the activation of hydrogen peroxide for the oxidation of organic substrates are triggered by enzymes called peroxidases.<sup>[18–20]</sup> Despite the efficiency of these enzymes in oxidizing phenolic or amine compounds, they present some limitations, including denaturation and high costs.<sup>[21]</sup>

In order to overcome such restraints, synthetic catalysts to oxidize phenolic and amine compounds using hydrogen peroxide have become an exciting alternative.

This paper reports the synthesis and characterization of a new series of zwitterionic cobalt complexes. The structural and electronic properties of the compounds were investigated using X-ray diffraction, UV–visible absorption spectroscopy, electrochemical analysis, and measurements of peroxidase activity.

## 2 | EXPERIMENTAL

### 2.1 | Materials and instrumentation

All manipulations were conducted by use of standard N<sub>2</sub> atmosphere. CHN elemental analyses were performed with a Shimadzu EA112 microanalysis instrument. <sup>1</sup>H NMR and <sup>13</sup>C NMR spectra were recorded with a Bruker DPX-400 spectrometer. DMSO-*d*<sub>6</sub> and CDCl<sub>3</sub> were used as the solvent and tetramethylsilane as the internal reference. Chemical shifts are reported in parts per million ( $\delta$ , ppm) and were referenced to residual solvent peak. Multiplicities are expressed as: s, singlet; t, triplet; q, quartet; quintet; sextet, m, multiplet; and br, broad. Fourier transform infrared (FT-IR) spectra were recorded using a Bruker Tensor 27 spectrometer with KBr pellets in the range 400–4000 cm<sup>-1</sup>. UV–visible absorption spectra were recorded with a Shimadzu UV-2600 spectrometer in dimethylformamide (DMF) solution. Cyclic voltammograms were recorded with a potentiostat/galvanostat (AutoLab EcoChemie PGSTAT

32N system) at room temperature and under argon atmosphere, in dry DMF solution. Electrochemical-grade tetrabutylammonium hexafluorophosphate (TBAPF<sub>6</sub>; 0.1 M) was used as supporting electrolyte. A standard three-component system was employed to carry out these cyclic voltammetry experiments with a glassy carbon working electrode, a platinum wire auxiliary electrode, and a platinum wire pseudo-reference electrode. To monitor the reference electrode, the ferrocenium/ferrocene redox couple was used as an internal reference.<sup>[22]</sup>

GC-MS analyses were performed using a Shimadzu QP2010PLUS GC-MS combination (Shimadzu Instruments). The GC was equipped with a low-polarity (5% phenylsiloxane, 95% methylsiloxane) capillary column (30 m length, 0.25 mm inner diameter, 0.25  $\mu$ m film thickness). Samples were dissolved in ethyl acetate at a concentration of 3 mg ml<sup>-1</sup> and injected into the instrument with an autosampler. The injector temperature was maintained at 250°C and the transfer interface at 280°C. The oven temperature was ramped from 50 to 250°C at a rate of 15°C min<sup>-1</sup>. The QP2010PLUS is an electron ionization quadrupole-based mass spectrometer with a maximum scan range of 900 amu and an ionizing electron energy of 70 eV.

### 2.2 | X-ray crystallography

Data were collected using a Bruker D8 Venture Photon 100 diffractometer equipped with an Incoatec I $\mu$ S high brilliance Mo K $\alpha$  X-ray tube with two-dimensional Montel micro-focusing optics. The structure was solved by direct methods using SHELXS.<sup>[23]</sup> Subsequent Fourier-difference map analyses yielded the positions of the non-hydrogen atoms. Refinements were carried out with the SHELXL package.<sup>[23]</sup> All refinements were made by full-matrix least-squares on  $F^2$  with anisotropic displacement parameters for all non-hydrogen atoms. Hydrogen atoms were included in the refinement in calculated positions but the atoms (of hydrogen) that are involved in special bond were located in the Fourier map. Visualization was done using DIAMOND for Windows.<sup>[24]</sup> Crystal data and more details of the data collection and refinements of complexes ZW2C, ZW3C and ZW4C are presented in Table 1.

### 2.3 | Peroxidase activity

#### 2.3.1 | Phenol substrate

Peroxidase activity was spectrophotometrically measured by monitoring the absorbance relative to the adduct phenol-(4-aminoantipyrene) chromophore at 510 nm<sup>[25]</sup>

**TABLE 1** Crystal data and structure refinement for ZW2C, ZW3C and ZW4C

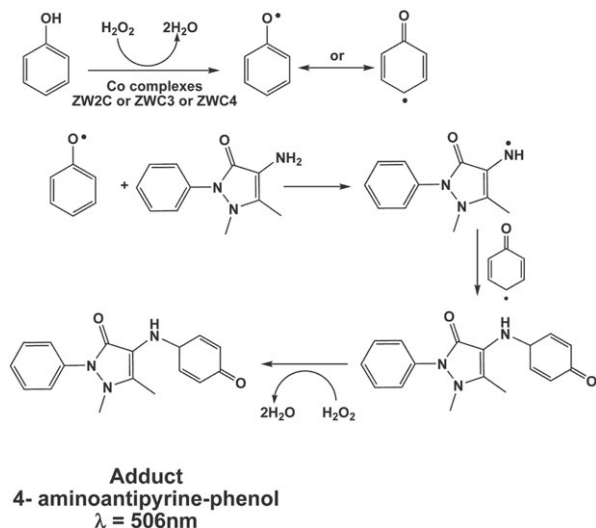
	ZW2C	ZW3C	ZW4C
Empirical formula	C <sub>32</sub> H <sub>34</sub> Cl <sub>3</sub> Co <sub>2</sub> N <sub>4</sub> O <sub>4</sub> S <sub>2</sub>	C <sub>36</sub> H <sub>41</sub> Cl <sub>3</sub> Co <sub>2</sub> N <sub>5</sub> O <sub>4</sub> S <sub>2</sub>	C <sub>40</sub> H <sub>45</sub> Cl <sub>3</sub> Co <sub>2</sub> N <sub>6</sub> O <sub>5</sub> S <sub>2</sub>
Formula weight	826.96	896.07	978.15
<i>T</i> (K)	100(2)	100(2)	100(2)
Radiation, $\lambda$ (Å)	Mo K $\alpha$ ; 0.71073	Mo K $\alpha$ ; 0.71073	Mo K $\alpha$ ; 0.71073
Crystal system, space group	Monoclinic, <i>P</i> <sub>2</sub> <sub>1</sub> / <i>c</i>	Monoclinic, <i>P</i> <sub>2</sub> <sub>1</sub> / <i>n</i>	Monoclinic, <i>C</i> 2/ <i>c</i>
Unit cell dimensions <i>a</i> (Å)	10.8177(2)	11.6726(19)	22.019(4)
<i>b</i> (Å)	20.2118(4)	16.855(3)	14.120(3)
<i>c</i> (Å)	16.9884(4)	20.913(4)	29.062(6)
$\alpha$ (°)	90	90	90.00(3)
$\beta$ (°)	91.6250(10)	101.585(6)	95.49(3)
$\gamma$ (°)	90	90	90.00(3)
<i>V</i> (Å <sup>3</sup> )	3712.94(13)	4030.6(12)	8994(3)
<i>Z</i> , calculated density (g cm <sup>-3</sup> )	4, 1.479	4, 1.477	8, 1.445
Absorption coefficient (mm <sup>-1</sup> )	1.262	1.170	1.057
<i>F</i> (000)	1692	1844	4032
Crystal size (mm)	0.484 × 0.241 × 0.132	0.292 × 0.257 × 0.143	0.230 × 0.168 × 0.072
Theta range for data collection	2.02–27.16	2.33–29.55	2.28–30.59
Index ranges	–12 < = <i>h</i> < =13 –25 < = <i>k</i> < =25 –21 < = <i>l</i> < =21	–16 < = <i>h</i> < =13 –19 < = <i>k</i> < =23 –13 < = <i>l</i> < =28	–31 < = <i>h</i> < =31 –20 < = <i>k</i> < =19 –41 < = <i>l</i> < =33
Reflections collected/unique	51780/8227	18767/11260	50093/13759
Completeness to theta max.	99.9%	99.8%	99.7%
Absorption correction	Multi-scan	Multi-scan	Multi-scan
Max. and min. transmission	0.9766 and 0.8859	0.800 and 0.862	0.801 and 0.862
Refinement method	Full-matrix least-squares on <i>F</i> <sup>2</sup>	Full-matrix least-squares on <i>F</i> <sup>2</sup>	Full-matrix least-squares on <i>F</i> <sup>2</sup>
Data/restraints/parameters	8227/0/412	11260/0/470	13759/2/537
Goodness-of-fit on <i>F</i> <sup>2</sup>	1.107	1.013	1.046
Final <i>R</i> indices [ <i>I</i> > 2 $\sigma$ ( <i>I</i> )]	<i>R</i> 1 = 0.0637, w <i>R</i> 2 = 0.1839	<i>R</i> 1 = 0.0706, w <i>R</i> 2 = 0.1442	<i>R</i> 1 = 0.0686, w <i>R</i> 2 = 0.1985
<i>R</i> indices	<i>R</i> 1 = 0.0837, w <i>R</i> 2 = 0.1984	<i>R</i> 1 = 0.1841, w <i>R</i> 2 = 0.1917	<i>R</i> 1 = 0.0965, w <i>R</i> 2 = 0.2171
Largest diff. peak and hole (e Å <sup>-3</sup> )	0.234 and –0.493	0.071 and –0.379	0.361 and –0.245

and 506 nm.<sup>[26]</sup> A modified methodology of Fontana and co-workers<sup>[27]</sup> (Scheme 1) was used. Phenol and 4-aminoantipyrine stock solutions were made by dissolving the corresponding masses in a 1 mM phosphate buffer solution (pH 7.0). Solutions of the 1.45 mM complexes (and ligands) were made in DMF and calibrated spectrophotometrically. The reactants were added to a quartz cuvette in order for the concentration of the reactants at the start of the reaction to be phenol 2.58 mM, 4-aminoantipyrine 1.05 mM, hydrogen peroxide 9.95 mM, and complex (or ligand) 9.65 mM. The start of the

reaction was timed after the addition of hydrogen peroxide. The reaction was conducted at room temperature in the absence of light. A blank experiment was performed in the absence of catalyst (complex or ligand).

### 2.3.2 | 3,5,3',5'-Tetramethylbenzidine (TMB) substrate

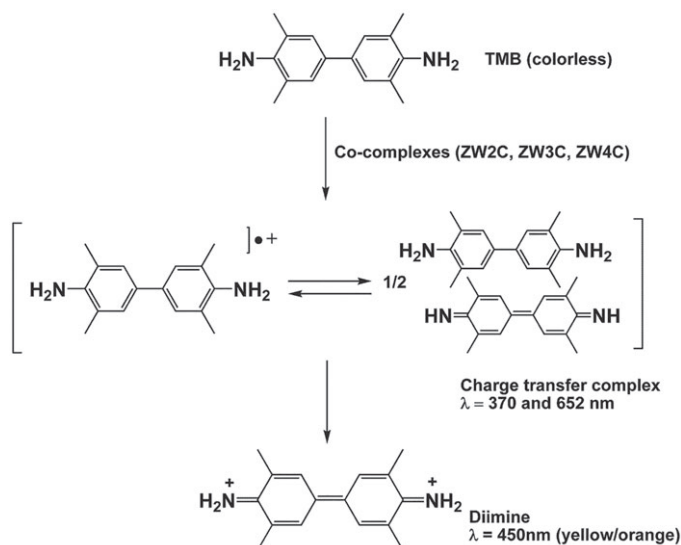
The substrate used for mimetic evaluation of peroxidase was TMB, which generates the yellow-colored oxidized



**SCHEME 1** Schematic representation of stabilization of the adduct 4-aminoantipyrine-phenol. Scheme adapted from Kim and collaborators<sup>[45]</sup>

TMB product (di-iminic molecule) when in contact with hydrogen peroxide and a catalyst. The absorbance was spectrophotometrically monitored at 450 nm.<sup>[28–30]</sup>

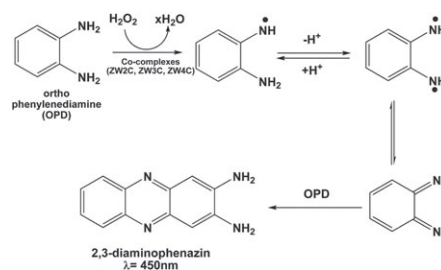
The stock solution of TMB was prepared using 0.056 g (2.3 mM) of TMB diluted in 2.5 ml of DMF and 2.5 ml of acetic acid, followed by the addition of 50  $\mu\text{L}$  of a KI solution (5 mM). The hydrogen peroxide solution was prepared using a concentration of 10 mM. The blank experiment was run in the absence of a catalyst (complex or ligand) with ethanol. The reagents were added to a quartz cuvette at a final ratio of 3 ml ethanol, 50  $\mu\text{L}$  (0.77 mM) TMB stock solution, 50  $\mu\text{L}$  (0.72 mM) hydrogen peroxide, and 30  $\mu\text{L}$  (3.78 mM) of catalyst (Scheme 2).



**SCHEME 2** Schematic representation of stabilization of the diimine form of the TMB substrate. Scheme adapted from the literature<sup>[15,65]</sup>

### 2.3.3 | *ortho*-Phenylenediamine (OPD) substrate

OPD is a water-soluble compound used as a substrate to evaluate the mimetic peroxidase activity of cobalt complexes. In contact with hydrogen peroxide and a catalyst, this initial substrate produces an orange/yellow-colored product (formation of 2,3-diaminophenazine (DAP) is spectrophotometrically monitored at 450 nm).<sup>[17,31,32]</sup> To obtain the buffer solution, 0.6 g of  $\text{Na}_2\text{HPO}_4$  (anhydrous; 8.45 mM), 0.11 g of  $\text{NaH}_2\text{PO}_4 \cdot \text{H}_2\text{O}$  (1.59 mM), and 4.3 g of NaCl (0.15 M) were added to 500 ml of distilled water. The OPD stock solution was prepared using 0.5 mg of the compound in 1 ml of buffer solution and 10  $\mu\text{L}$  of sulfuric acid (2.0 M). For the hydrogen peroxide solution, 50  $\mu\text{L}$  of  $\text{H}_2\text{O}_2$  was used in 5 ml of distilled water. The blank experiment was performed in the absence of catalyst (complex or ligand) with distilled water. The reagents were added to a cuvette for the final concentrations of 3 ml of distilled water, 0.92 mM OPD stock solution, 0.14 mM hydrogen peroxide, and 3.78 mM catalyst (3.8 mM) (Scheme 3).



**SCHEME 3** Schematic representation of the diaminophenazine obtained from the initial substrate OPD. Scheme adapted from the literature<sup>[66,67]</sup>

## 2.4 | Synthetic procedures

### 2.4.1 | Ligand synthesis: general procedure

#### General procedure for *S*-alkylation of 2-aminothiophenol

2-Aminothiophenol (0.250 g, 2.0 mmol) was dissolved in anhydrous methanol (15 ml) and KOH (0.112 g, 2.0 mmol) was added. The bright yellow solution was stirred during 30 min under N<sub>2</sub> atmosphere. After this period, a methanolic solution (10 ml) containing 2.0 mmol of the corresponding alkyl halide (ethyl, propyl, or butyl) was added dropwise, and the reaction mixture was stirred at room temperature for 3 h. After this period, the methanol was evaporated and the reaction extracted with dichloromethane (3 × 25 ml). The dichloromethane was evaporated, and the resulting oil was dissolved in methanol (10 ml) and treated with concentrated hydrochloric acid (to pH 2.0). The solvent was evaporated, and the resulting solid was washed three times with diethyl ether (15 ml). It was then recrystallized from methanol (20 ml) to afford a white-gray solid.

2-(Ethylthio)benzenamine hydrochloridate. Yield: 68%. Anal. Calcd for C<sub>8</sub>H<sub>12</sub>NSCl (%): C 50.65; H 6.38; N 7.38. Found (%): C 50.66; H 6.35; N 7.34. M.p. 157–158°C. FT-IR (KBr pellets, cm<sup>-1</sup>): 751.1 [m, ν(C—S)], 2846 [s, ν(C—NH<sub>3</sub><sup>+</sup>)], 1507 [m, ν(C—NH<sub>3</sub><sup>+</sup>)], 1558 [m, ν(C=C<sub>ar</sub>)]. <sup>1</sup>H NMR (400 MHz, DMSO-*d*<sub>6</sub>, δ in ppm): 1.19 (t, CH<sub>3</sub>, 3H), 2.94 (q, CH<sub>2</sub>, 2H), 5.54 (br, C—NH<sub>3</sub><sup>+</sup>, 3H), 7.21 (m, C—H<sub>ar</sub>, 1H), 7.30 (m, C—H<sub>ar</sub>, 1H), 7.44 (m, C—H<sub>ar</sub>, 1H), 7.53 (m, C—H<sub>ar</sub>, 1H). <sup>13</sup>C NMR (400 MHz, DMSO-*d*<sub>6</sub>, δ in ppm): 14.59 (CH<sub>3</sub>), 28.90 (CH<sub>2</sub>), 122.51 (C<sub>ar</sub>), 126.38 (C<sub>ar</sub>), 127.44 (C<sub>ar</sub>), 128.83 (C<sub>ar</sub>), 133.86 (C<sub>ar</sub>), 136.51 (C<sub>ar</sub>).

2-(Propylthio)benzenamine hydrochloridate. Yield: 83%. Anal. Calcd for C<sub>9</sub>H<sub>15</sub>NSCl (%): C 53.06; H 6.93; N 6.88. Found (%): C 53.00; H 6.92; N 6.82. M.p. 150–153°C. FT-IR (KBr pellets, cm<sup>-1</sup>): 748 [s, ν(C—S)], 2846 [s, ν(C—NH<sub>3</sub><sup>+</sup>)], 1473 [m, ν(C—NH<sub>3</sub><sup>+</sup>)], 1572 [m, ν(C=C<sub>ar</sub>)]. <sup>1</sup>H NMR (400 MHz, DMSO-*d*<sub>6</sub>, δ in ppm): 0.95 (t, CH<sub>3</sub>, 3H), 1.57 (sextet, CH<sub>2</sub>, 2H), 2.89 (t, CH<sub>2</sub>, 2H), 5.27 (br, C—NH<sub>3</sub><sup>+</sup>), 7.20 (m, C—H<sub>ar</sub>, 1H), 7.28 (m, C—H<sub>ar</sub>, 1H), 7.42 (m, C—H<sub>ar</sub>, 1H), 7.50 (m, C—H<sub>ar</sub>, 1H). <sup>13</sup>C NMR (400 MHz, DMSO-*d*<sub>6</sub>, δ in ppm): 13.47 (CH<sub>3</sub>), 22.47 (CH<sub>3</sub>—CH<sub>2</sub>), 36.82 (S—CH<sub>2</sub>), 122.25 (C<sub>ar</sub>), 126.32 (C<sub>ar</sub>), 127.92 (C<sub>ar</sub>), 128.52 (C<sub>ar</sub>), 133.51 (C<sub>ar</sub>), 136.30 (C<sub>ar</sub>).

2-(Butylthio)benzenamine hydrochloridate. Yield: 94%. Anal. Calcd for C<sub>10</sub>H<sub>16</sub>NSCl (%): C 55.16; H 7.41; N 6.43. Found (%): C 55.15; H 7.42; N 6.42. M.p. 141–143°C. FT-IR (KBr pellets, cm<sup>-1</sup>): 761 [m, ν(C—S)], 2854 [s, ν(C—NH<sub>3</sub><sup>+</sup>)], 1473 [m, ν(C—NH<sub>3</sub><sup>+</sup>)], 1557 [m,

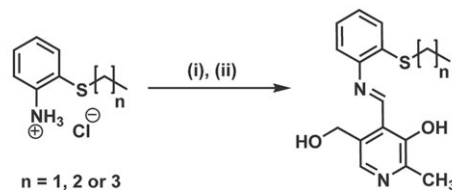
ν(C=C<sub>ar</sub>)]. <sup>1</sup>H NMR (400 MHz, DMSO-*d*<sub>6</sub>, δ in ppm): 0.86 (t, CH<sub>3</sub>, 3H), 1.37 (sextet, CH<sub>2</sub>, 2H), 1.52 (quintet, CH<sub>2</sub>, 2H), 2.93 (t, CH<sub>2</sub>, 2H), 5.31 (br, C—NH<sub>3</sub><sup>+</sup>, 3H), 7.24 (m, C—H<sub>ar</sub>, 1H), 7.30 (m, C—H<sub>ar</sub>, 1H), 7.45 (m, C—H<sub>ar</sub>, 1H), 7.53 (m, C—H<sub>ar</sub>, 1H). <sup>13</sup>C NMR (400 MHz, DMSO-*d*<sub>6</sub>, δ in ppm): 13.36 (CH<sub>3</sub>), 21.22 (CH<sub>2</sub>), 30.66 (CH<sub>2</sub>—CH<sub>2</sub>), 33.80 (CH<sub>2</sub>), 122.39 (C<sub>ar</sub>), 126.54 (C<sub>ar</sub>), 128.03 (C<sub>ar</sub>), 128.06 (C<sub>ar</sub>), 132.82 (C<sub>ar</sub>), 135.15 (C<sub>ar</sub>).

### 2.4.2 | General procedure for synthesis of Schiff bases

#### General procedure for ligands L2C, L3C, and L4C

Pyridoxal hydrochloride (0.224 g, 1.1 mmol) was dissolved in anhydrous methanol (10 ml). Thereafter, the respective amine (ethyl, propyl, or butyl) (0.189 g; 0.203 g; 0.217 g; 1 mmol each) was added and the mixture was refluxed at 70°C for 2 h. After this period, the reaction mixture was cooled to room temperature and KOH (0.118 g, 2.1 mmol) dissolved in methanol (5 ml) was added. The reaction was stirred at room temperature for a further 15 min. The methanol was then evaporated under reduced pressure and the solid washed three times with water (15 ml), three times with ethyl ether (15 ml), and three times with hexane (15 ml). The resulting solid was filtered, recrystallized from methanol, and dried in a desiccator (Scheme 4) and an orange crystalline substance was obtained.

Ligand L2C: 4-(2-(ethylthio)phenylimino)methyl-5-(hydroxymethyl)-2-methylpyridin-3-ol. Yield: 87%. Anal. Calcd for C<sub>16</sub>H<sub>18</sub>N<sub>2</sub>O<sub>2</sub>S (%): C 63.55; H 6.00; N 9.26. Found (%): C 63.52; H 6.02; N 9.25. M.p. 133–134°C. FT-IR (KBr pellets, cm<sup>-1</sup>): 750 [m, ν(C—S)], 1605 [m, ν(C=N)], 1581 [m, ν(C=C<sub>ar</sub>)], 1282 [f, ν(C—O<sub>ar</sub>)]. <sup>1</sup>H NMR (400 MHz, CDCl<sub>3</sub>, δ in ppm): 1.38 (t, CH<sub>3</sub>, 3H), 2.60 (s, CH<sub>3</sub>, 3H), 2.99 (q, S—CH<sub>2</sub>, 2H), 4.87 (s, CH<sub>2</sub>—O, 2H), 7.24 (m, C—H<sub>ar</sub>, 2H), 7.30 (m, C—H<sub>ar</sub>, 1H), 7.37 (m, C—H<sub>ar</sub>, 1H), 7.97 (s, C—H<sub>ar</sub>, 1H), 9.16 (s, C—H<sub>imine</sub>, 1H). UV-visible (DMF, λ<sub>max</sub> in nm; ε<sub>max</sub> in M<sup>-1</sup> cm<sup>-1</sup>): 276 (11 390). The X-ray crystal structure of the ligand is described in the supporting information.



(i) Pyridoxal hydrochloride, MeOH, reflux, 2 h. (ii) KOH, MeOH, 15 min

**SCHEME 4** Synthetic route of ligands L2C, L3C, and L4C through condensation reaction of pyridoxal with 2-aminothiophenol derivative

Ligand L3C: 4-(2-(propylthio)phenylimino)methyl-5-(hydroxymethyl)-2-methylpyridin-3-ol. Yield: 74%. Anal. Calcd for  $C_{17}H_{20}N_2O_2S$  (%): C 64.53; H 6.37; N 9.26. Found (%): C 64.58; H 6.44; N 8.77. M.p. 131–132°C. FT-IR (KBr pellets,  $cm^{-1}$ ): 754.4 [m,  $\nu$  (C—S)], 1606.7 [m,  $\nu$  (C=N)], 1582 [f,  $\nu$  (C=C<sub>ar</sub>)], 1286 [m,  $\nu$  (C—O<sub>ar</sub>)]. <sup>1</sup>H NMR (400 MHz, CDCl<sub>3</sub>,  $\delta$  in ppm): 1.08 (t, CH<sub>3</sub>, 3H), 1.77 (sextet, CH<sub>2</sub>—CH<sub>2</sub>, 2H), 2.61 (s, CH<sub>3</sub>, 3H), 2.96 (t, CH<sub>2</sub>—S, 2H), 4.88 (s, O—CH<sub>2</sub>, 2H), 7.25 (m, C—H<sub>ar</sub>, 2H), 7.31 (m, C—H<sub>ar</sub>, 1H), 7.39 (m, C—H<sub>ar</sub>, 1H), 7.93 (s, C—H<sub>ar</sub>, 1H), 9.19 (s, C—H<sub>imine</sub>, 1H). UV-visible (DMF,  $\lambda_{max}$  in nm;  $\epsilon_{max}$  in  $M^{-1} cm^{-1}$ ): 276 (13 363).

Ligand L4C: 4-(2-(butylthio)phenylimino)methyl-5-(hydroxymethyl)-2-methylpyridin-3-ol. Yield: 63%. Anal. Calcd for  $C_{18}H_{22}N_2O_2S$  (%): C 65.42; H 6.71; N 8.48. Found (%): C 65.44; H 6.77; N 8.40. M.p. 124–125°C. FT-IR (KBr pellets,  $cm^{-1}$ ): 753.6 [m,  $\nu$  (C—S)], 1607 [m,  $\nu$  (C=N)], 1582 [m,  $\nu$  (C=C<sub>ar</sub>)], 1287 [m,  $\nu$  (C—O<sub>ar</sub>)]. <sup>1</sup>H NMR (400 MHz, CDCl<sub>3</sub>,  $\delta$  in ppm): 0.96 (t, CH<sub>3</sub>, 3H), 1.52 (sextet, CH<sub>2</sub>—CH<sub>2</sub>—CH<sub>3</sub>, 2H), 1.72 (quintet, S—CH<sub>2</sub>, 2H), 2.62 (s, CH<sub>3</sub>, 3H), 2.98 (t, CH<sub>2</sub>—S, 2H), 4.88 (s, O—CH<sub>2</sub>, 2H), 7.25 (m, C—H<sub>ar</sub>, 2H), 7.31 (m, C—H<sub>ar</sub>, 1H), 7.40 (m, C—H<sub>ar</sub>, 1H), 7.96 (s, C—H<sub>ar</sub>, 1H), 9.18 (s, C—H<sub>imine</sub>, 1H). UV-visible (DMF,  $\lambda_{max}$  in nm;  $\epsilon_{max}$  in  $M^{-1} cm^{-1}$ ): 274 (16 769).

### 2.4.3 | Synthesis of complexes ZW2C, ZW3C, and ZW4C

For the synthesis of these complexes, the reactions were conducted *in situ*. In a round-bottom flask containing acetonitrile (20 ml) were added pyridoxal (0.20 mmol) and the corresponding amine (0.20 mmol). The resulting mixture was heated to 70°C and kept under magnetic stirring for 30 min. After this period, upon the addition of trimethylamine, an intense yellow coloration formed which changed to dark brown upon addition of CoCl<sub>2</sub>·6H<sub>2</sub>O (0.20 mmol). The resulting mixture was kept under magnetic stirring for 3 h at 70°C. After the reaction, the solution was filtered, and allowed to stand for five days, with the slow evaporation of acetonitrile to form dark-red crystals (Scheme 5).

Complex ZW2C. Dark-red crystals. Yield: 57%. Anal. Calcd for  $C_{32}H_{34}N_4O_4S_2Cl_3Co_2$  (%): C 46.47; H 4.14; N

6.77. Found (%): C 46.57; H 4.16; N 6.64. M.p. >350°C (dec.). FT-IR (KBr pellets,  $cm^{-1}$ ): 766.5 [m,  $\nu$  (C—S)], 1604.3 [m,  $\nu$  (C=N)], 1573.7 [ $\nu$  (C=C<sub>ar</sub>)], 1270 [m,  $\nu$  (C—O<sub>ar</sub>)]. UV-visible (DMF,  $\lambda_{max}$  in nm;  $\epsilon_{max}$  in  $M^{-1} cm^{-1}$ ): 267 (50 144), 449 (11 143) and 490 (5571).

Complex ZW3C. Dark-red crystals. Yield: 46%. Anal. Calcd for  $C_{36}H_{41}N_5O_4S_2Cl_3Co_2$  (%): C 48.25; H 4.61; N 7.82. Found (%): C 48.57; H 4.66; N 7.54. M.p. >350°C (dec.). FT-IR (KBr pellets,  $cm^{-1}$ ): 765.7 [m,  $\nu$  (C—S)], 1604.5 [m,  $\nu$  (C=N)], 1573.8 [ $\nu$  (C=C<sub>ar</sub>)], 1271.5 [m,  $\nu$  (C—O<sub>ar</sub>)]. UV-visible (DMF,  $\lambda_{max}$  in nm;  $\epsilon_{max}$  in  $M^{-1} cm^{-1}$ ): 267 (66 092), 448 (14 687) and 489 (7343).

Complex ZW4C. Dark-red crystals. Yield: 63%. Anal. Calcd for  $C_{40}H_{45}N_6O_5S_2Cl_3Co_2$  (%): C 48.86; H 5.13; N 8.55. Found (%): C 48.80; H 5.39; N 8.54. M.p. >350°C (dec.). FT-IR (KBr pellets,  $cm^{-1}$ ): 768.9 [m,  $\nu$  (C—S)], 1602.8 [m,  $\nu$  (C=N)], 1573.5 [ $\nu$  (C=C<sub>ar</sub>)], 1271.7 [m,  $\nu$  (C—O<sub>ar</sub>)]. UV-visible (DMF,  $\lambda_{max}$  in nm;  $\epsilon_{max}$  in  $M^{-1} cm^{-1}$ ): 271 (42 323), 450 (9405) and 490 (4702).

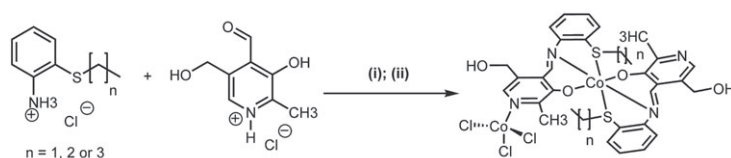
## 2.5 | Computational details

Density functional theory was used to determine the Fukui indices associated with the ZW2C, ZW3C, and ZW4C complexes. Before calculating the Fukui indices, the molecular structures of these three compounds were optimized, using as starting configurations the X-ray crystallographic data for these compounds (see Section 4.1). The exchange and correlation contributions were described by the hybrid B3LYP functional. The molecular orbitals were represented by linear combinations of relativistic effective-core-potential double-zeta quality basis sets.<sup>[33]</sup> All calculations were done using the Gaussian 09 code.<sup>[34]</sup> The charge density plots associated with the local Fukui functions were obtained using the Chemcraft program.<sup>[35]</sup>

## 3 | RESULTS AND DISCUSSION

### 3.1 | Crystal structures of ZW2C, ZW3C, and ZW4C

The three cobalt complexes synthesized have the same coordination environments, which are usually octahedral Co(III) coordinated to O (phenolate), N



(i) MeCN, 30 min, 70 °C; (ii) Et<sub>3</sub>N, CoCl<sub>2</sub>·6H<sub>2</sub>O, 3h, 70°C.

**SCHEME 5** *In situ* synthetic route of cobalt complexes ZW2C, ZW3C, and ZW4C

(azomethine), and S (thioether) atoms. On the other hand, the Co(II) ion presents tetrahedral geometry coordinating to the N (pyridine) from the pyridoxal and three chlorides (Table 2 presents the principal bond lengths and angles of the complexes). An ORTEP representation of the structures of the three complexes is shown in Figure 1.

The octahedral cobalt ion has a coordination sphere formed by two mono-anionic ligands. Three anionic chlorides and the pyridine nitrogen of one of the ligands (pyridoxal derivative) coordinate to the tetrahedral cobalt ion. Thus, considering the bonding distances and strong tendency of Co(II) ions to adopt tetrahedral geometry, it is possible to conclude that there is a negative charge on this atom due to the coordination of three chlorine atoms. However, the octahedral cobalt ion is Co(III) species, with a positive charge remaining on this atom due to the coordination of only two anionic ligands (phenolates). Thus, the complexes can have a zwitterionic nature, with a negative charge on the tetrahedral cobalt atom and a positive charge on the octahedral cobalt atom, which makes the complex neutral. Lengths and angles for the X-ray structural parameter analysis of complexes ZW2C, ZW3C, and ZW4C are presented in Table 3.

**TABLE 2** Distances for Co<sup>III</sup>-N (imine), Co<sup>III</sup>-O (phenolate), Co<sup>III</sup>-S (thiolate), Co<sup>III</sup>-S (thioether), Co<sup>III</sup>-S (thiolate) $\mu$ , Co<sup>II</sup>-Cl and Co<sup>II</sup>-N (pyridine) and their respective references

Metal and Lewis Base	Bond (Å)	Ref.
Co <sup>III</sup> -N (imine)	1.946(3)	[32]
	2.046(3)	
	1.913(3)	[60]
	1.926(2)	
	1.93	[61]
	1.858 (7)	[62]
Co <sup>III</sup> -O (phenolate)	1.923(5)	[63]
	1.894(2)	[60]
	1.914(2)	
	1.93	[61]
Co <sup>III</sup> -S (thiolate)	1.898(5)	[63]
	2.217(3)	[32]
	1.927(3)	
Co <sup>III</sup> -S (thioether)	2.227	[60]
	2.2017(16)	[32]
	2.221(3)	
	2.238	[60]
Co <sup>III</sup> -S (thiolate) $\mu$	2.196(2)	[63]
	2.3156	[62]
Co <sup>II</sup> -Cl	2.28	[61]
	2.227(2)	[63]
Co <sup>II</sup> -N (pyridine)	2.126(4)	[64]
	2.138(4)	

Based on crystalline packing, it is possible to identify centrosymmetric dimer formation in the structures of complexes ZW2C and ZW3C (Figure 2). Each hydrogen atom of each of the alcohol functions makes a strong hydrogen bond<sup>[36,37]</sup> with a nitrogen atom of the pyridine unit. The ZW2C complex forms two equivalent hydrogen bonds with N (pyridinium)⋯H—O (alcohol) bond distance equal to 2.799 Å. The ZW3C complex forms an analogue dimer with N (pyridinium)⋯H—O (alcohol) and bond distance equal to 2.796 Å (Table 4).

The other oxygen atom of the alcohol function (O4) of the pyridoxal makes hydrogen bonds with electronegative atoms (three chloride ions) coordinated to the Co(II) ions (Figure 3).

### 3.2 | UV-visible absorption analysis

The absorption spectra of the ligands are shown in the supporting information. The bands are observed around 276 and 364 nm, which can be attributed to the intraligand transition bands  $\pi \rightarrow \pi^*$  and  $n \rightarrow \pi^*$ , respectively.<sup>[38–41]</sup> Electronic transition bands between 400 and 550 nm are observed for cobalt complexes ZW2C, ZW3C, and ZW4C, which can be attributed to ligand-to-metal charge transfer transitions that involve the oxygen of the phenolate ( $\text{PhO}^- \rightarrow \text{Co(III)}$ )<sup>[42]</sup> (Figure 4; Table 5). A low-intensity band (shoulder) was observed in the region between 600 and 700 nm, which may be attributable to a d-d type transition.<sup>[43]</sup> The fact that these Co complexes present Co(II) ions in a tetrahedral environment suggests that lower energy transitions probably occur based on Laporte/spin rules. Another plausible explanation is that the solvent (DMF) may coordinate with tetrahedral Co(II) species and change its coordination geometry, possibly to an octahedral environment.

### 3.3 | Density functional theory results

To better understand the electronic nature of the zwitterionic cobalt complexes, the Fukui functions have been determined associated with electronic densities according to the following equations:

$$F+(r) = \rho_{N+1}(r) - \rho_N(r)$$

$$F-(r) = \rho_N(r) - \rho_{N-1}(r)$$

where  $F+$  and  $F-$  are the Fukui functions for the electrophilic and nucleophilic regions of these complexes, the electronic charge for a molecule with  $X$  electrons.

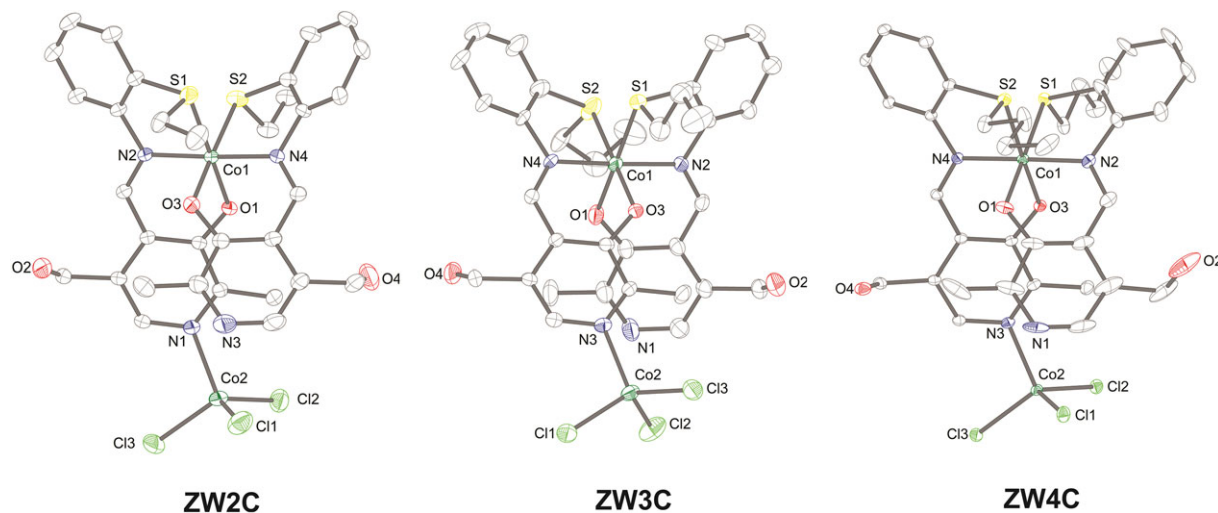


**FIGURE 1** Structural representation of complexes ZW2C, ZW3C, and ZW4C with 50% ellipsoids. Hydrogen atoms and crystallization solvates are omitted for better visualization of the structure

**TABLE 3** Bond lengths and angles for complexes ZW2C, ZW3C, and ZW4C

Atoms	Bond length (Å)			Atoms	Angle (°)		
	ZW2C	ZW3C	ZW4C		ZW2C	ZW3C	ZW4C
Co1–O3	1.879(3)	1.880(3)	1.874(3)	O3–Co1–O1	88.48(12)	88.15(15)	90.14(14)
Co1–O1	1.890(3)	1.884(3)	1.882(3)	O3–Co1–N4	92.53(14)	93.78(15)	92.43(14)
Co1–N4	1.907(3)	1.916(4)	1.923(3)	O1–Co1–N4	88.80(13)	89.19(17)	87.08(15)
Co1–N2	1.926(3)	1.932(5)	1.918(4)	O3–Co1–N2	89.49(13)	86.63(16)	86.40(14)
Co1–S1	2.2603(12)	2.2623(15)	2.2540(12)	O1–Co1–N2	92.55(13)	93.30(18)	92.77(16)
Co1–S2	2.2718(13)	2.2647(16)	2.2478(12)	N4–Co1–N2	177.60(13)	177.49(18)	178.82(15)
Co2–Cl1	2.2419(16)	2.248(2)	2.2551(14)	O3–Co1–S1	91.69(10)	92.67(11)	91.93(10)
Co2–Cl2	2.2603(14)	2.2696(17)	2.2718(14)	O1–Co1–S1	179.29(10)	179.17(12)	177.90(10)
Co2–Cl3	2.2758(16)	2.2767(17)	2.2541(13)	N4–Co1–S1	91.88(11)	90.68(12)	93.18(11)
Co2–N1	2.078(3)	—	—	N2–Co1–S1	86.76(10)	86.83(14)	87.01(12)
Co2–N3	—	2.070(4)	2.066(3)	O3–Co1–S2	178.29(10)	178.58(13)	176.42(10)
				O1–Co1–S2	91.52(9)	90.65(12)	93.43(11)
				N4–Co1–S2	85.77(11)	86.97(12)	88.02(11)
				N2–Co1–S2	92.21(10)	92.67(12)	93.16(11)
				S1–Co1–S2	88.33(5)	88.52(7)	84.50(5)
				Cl1–Co2–Cl2	114.96(6)	110.13(7)	112.36(5)
				Cl1–Co2–Cl3	110.22(7)	109.73(6)	113.53(5)
				Cl2–Co2–Cl3	109.10(6)	111.04(8)	109.03(5)
				N1–Co2–Cl1	105.48(11)	—	—
				N1–Co2–Cl2	110.93(10)	—	—
				N1–Co2–Cl3	105.74(11)	—	—
				N3–Co2–Cl1	—	104.82(14)	104.93(10)
				N3–Co2–Cl2	—	107.84(13)	111.10(11)
				N3–Co2–Cl3	—	113.10(12)	105.65(11)

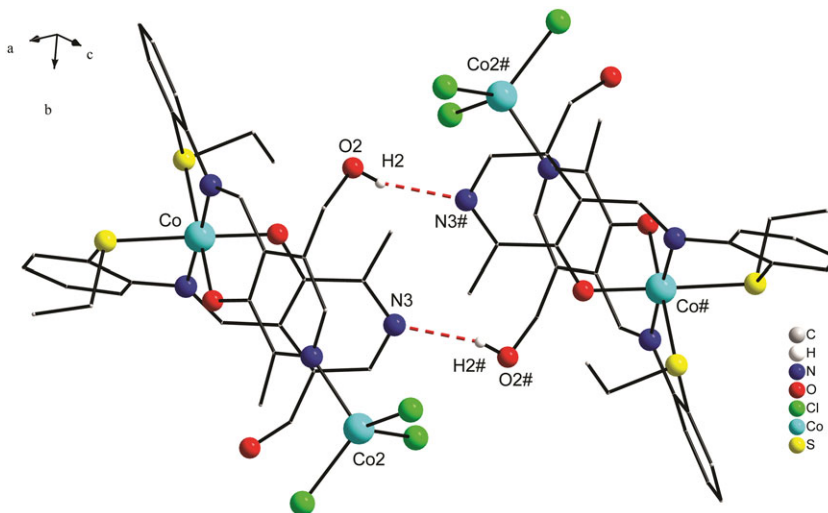


**FIGURE 2** Hydrogen bonds of complex ZW2C at the crystallographic plane *ac*. The crystallization solvates and hydrogens not involved in the hydrogen bonds are omitted

**TABLE 4** Lengths and angles of hydrogen bonds characterized as strong according to the adopted parameters<sup>[36,37]</sup>

(D-H...A)	D-H (Å)	H...A (Å)	D...A (Å)	D-H...A (°)
ZW2C O-H...N	0.820(5)	2.136(5)	2.799(6)	137.91(26)
ZW3C O-H...N	0.820(5)	2.016(5)	2.796(8)	158.53 (32)

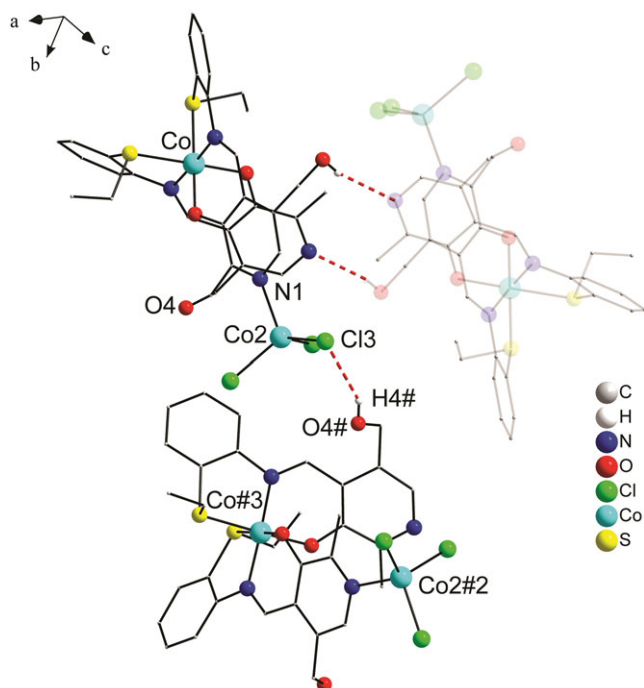


**FIGURE 3** Hydrogen bonds in complex ZW2C along the direction [010]. The crystallization solvates and hydrogen atoms not involved in the hydrogen bonds are omitted

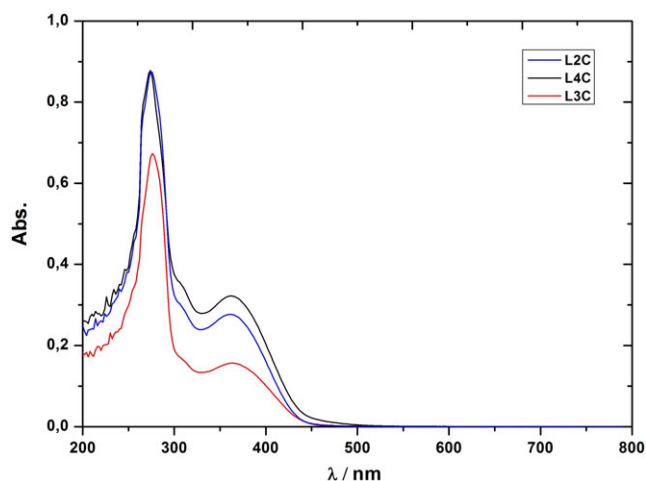


**FIGURE 4** UV-visible absorption spectra of cobalt complexes ZW2C, ZW3C, and ZW4C in DMF solution ( $10^{-5}$  M)

The electronic charge densities for the positive and negative specimens of these three complexes,  $\rho_{N-1}(r)$  and  $\rho_{N+1}(r)$  respectively, have been determined through static self-consistent field electronic structure calculations using

**TABLE 5** UV–visible transition band data of free ligands (L2C, L3C, L4C) and Co complexes (ZW2C, ZW3C, ZW4C)

Compound	nm ( $\epsilon$ , $M^{-1} \text{ cm}^{-1}$ )
L2C	276 (11 390)
L3C	276 (13 363)
L4C	274 (16 769)
ZW2C	267 (50 144), 449 (11 143) and 490 (5571)
ZW3C	268 (66 092), 448 (14 687) and 489 (7343)
ZW4C	271 (2323), 450 (9405) and 490 (4702)

the same minimum energy configurations obtained for the systems with  $N$  electrons.

The chemically active regions of these are qualitatively described by the nucleophilic property,  $F^-(r)$ , Fukui functions. The nucleophilic regions for the ZW2C, ZW3C, and ZW4C complexes are presented in Figure 9.

From Figure 5, it can be clearly seen that the Co(II) sites will always behave as nucleophilic active regions, irrespective of the considered complex. On the other hand, the Co(III) centers exhibit different nucleophilic activities. For example, for the ZW3C molecule, the Fukui function of Co(III) species shows no activity. Further, in ZW4C complex, Co(II) units are seen to have a greater nucleophilic activity among the three complexes.

Finally, the Fukui function by theoretical calculation analysis suggests that the Co(III) ions show some nucleophilic activity in the ZW2C complex, although less than in complex ZW4C. These qualitative results indicate that the ZW4C cobalt derivative will show a stronger nucleophilic activity, when compared to the ZW2C and ZW3C complexes, due to the greater chemical reactivity of the

peripheral tetrahedral Co(II) units, which corroborates and give theoretical support to the experimental evidences.

### 3.4 | Cyclic voltammetry analysis

The electrochemical behavior of the Co complexes was investigated using cyclic voltammetry with a platinum electrode (working electrode) in a dry DMF solution in the range 1.0 to 2.0 mM and with 0.1 M TBAPF<sub>6</sub> as the supporting electrolyte. This was performed in an argon-saturated atmosphere in the potential range  $-2.00$  to  $+1.50$  V versus NHE (Figure 6; Table 6). In general, the ligands presented an irreversible oxidation process in the anodic region. This can be attributed to the oxidation of the sulfur atom, which likely forms sulfoxide (SO) species in solution. In the negative region, only one reduction process was observed, which can be assigned to the imine group.<sup>[44]</sup>

For the complexes, zwitterionic cobalt species present two reduction processes in the cathodic region. The first reduction can be attributed to the Co<sup>III</sup>/Co<sup>II</sup> reduction process of the octahedral center,<sup>[42,45]</sup> leading to the second process, which can be assigned to the ligand reduction process. In the positive region, all complexes presented an irreversible anodic peak, which can be attributed to the oxidation of tetrahedral Co(II) units, forming the Co<sup>II</sup>/Co<sup>III</sup> redox couple.<sup>[46]</sup> Additionally, oxidation and reduction processes of cobalt ion revealed that the redox behavior of zwitterionic Schiff base complexes involves one-electron transfer reaction each (confirmed by coulometric analysis; see supporting information).

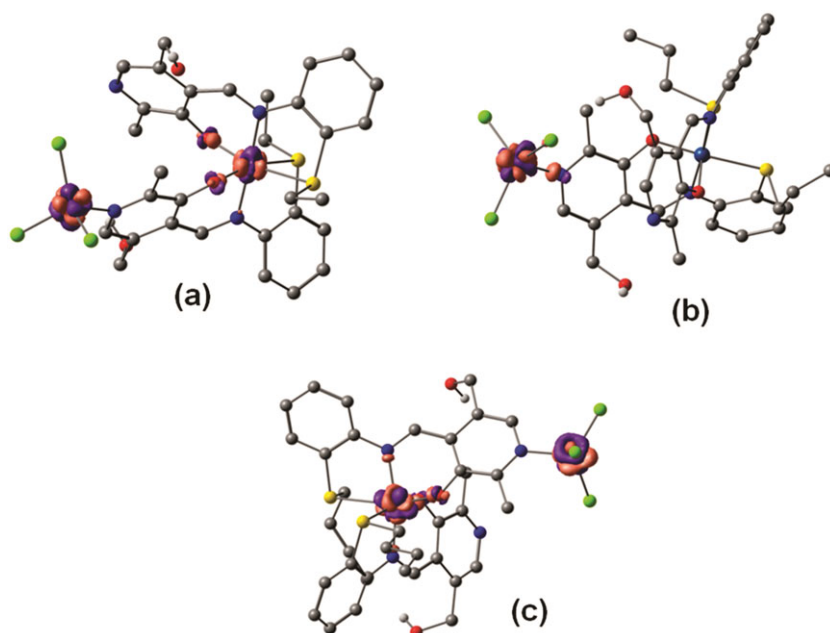


**FIGURE 5** Nucleophilic Fukui functions for cobalt complexes (a) ZW2C, (b) ZW3C, and (c) ZW4C. The figures shown in (a–c) have been obtained using the same isosurface value of  $0.04 \text{ e } A^{-3}$

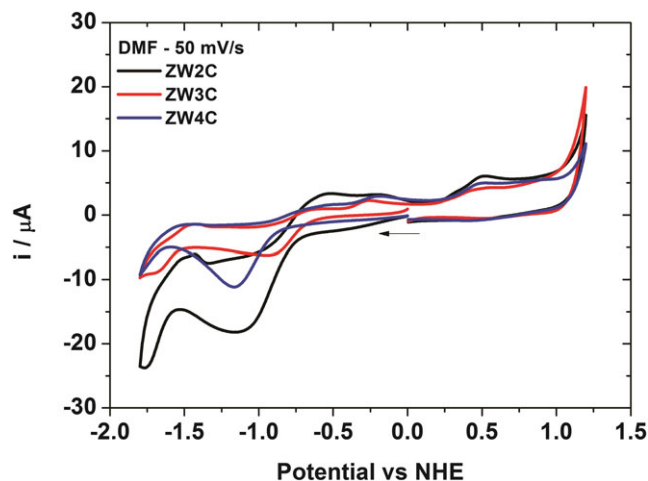


**FIGURE 6** Cyclic voltammetry of dinuclear cobalt complexes ZW2C, ZW3C, and ZW4C using 0.1 M TBAPF<sub>6</sub> as support electrolyte and scan rate of 50 mV s<sup>-1</sup>

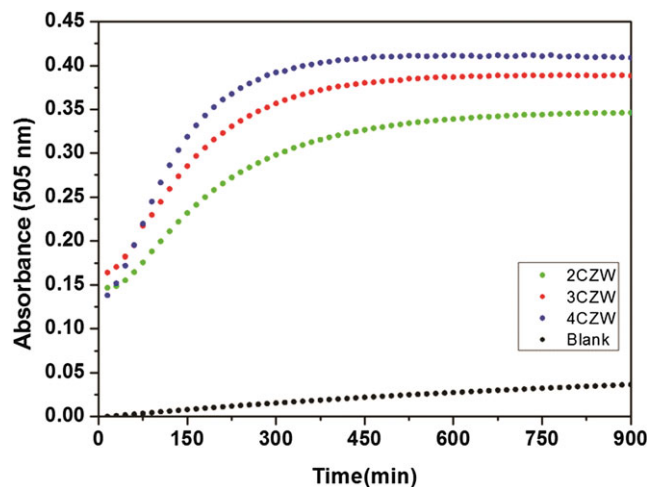


**FIGURE 7** Absorbance graphs for the reaction phenol + 4-aminoantipyrene + hydrogen peroxide + catalyst after 900 min of reaction

**TABLE 6** Summary of redox potential of free ligands and zwitterionic Co complexes

Compound	$E_1$ (V)	$E_2$ (V)	$E_3$ (V)
L2C	+0.606 <sup>a</sup>	-0.868 <sup>b</sup>	—
L3C	+0.632 <sup>a</sup>	-0.819 <sup>b</sup>	—
L4C	+0.648 <sup>a</sup>	-0.952 <sup>b</sup>	—
ZW2C	+0.505 <sup>a</sup>	-0.554 <sup>a</sup>	-1.136 <sup>b</sup>
ZW3C	+0.437 <sup>a</sup>	-0.276 <sup>a</sup>	-0.902 <sup>b</sup>
ZW4C	+0.483 <sup>a</sup>	-0.189 <sup>a</sup>	-1.161 <sup>b</sup>

<sup>a</sup> $E_{pa}$  = anodic peak.

<sup>b</sup> $E_{pc}$  = cathodic peak.

## 4 | PEROXIDASE MIMETIC ASSAYS

### 4.1 | Phenol substrate

Complexes and ligands were investigated for their ability to activate hydrogen peroxide for phenol oxidation. Thus, the reaction between phenol and 4-aminoantipyrene was monitored spectrophotometrically at 505 nm in order to quantify the formation of phenol-(4-aminoantipyrene) chromophore (confirmed by GC-MS analyses; see supporting information). The absorption plots in the region 400 to 700 nm obtained after 15 h of reaction are shown in Figure 7. These results allowed us to draw a general profile of the peroxidase activity of the compounds synthesized in this study and correlate it with the structure of the complexes obtained.

Ligands (L2C, L3C, and L4C) had no peroxidase activity. This is because the amount of the

phenol-4-aminoantipyrene chromophore formed was very similar to the blank.

The results obtained using cobalt complexes were similar to those reported by Kim and co-workers,<sup>[47]</sup> who used copper(II) perchlorate hexahydrate as a catalyst. On the other hand, when comparing the results obtained with those reported by Xiong and collaborators,<sup>[48]</sup> the mixed-valence complexes did not have the same efficiency in aminoantipyrene-phenol adduct formation. Moreover, it is possible that the reaction mechanism depends on the formation of peroxide bonds with the cation, which is disadvantageous in complexes with octahedral coordination geometry, in addition to external sphere mechanisms not being effective for these types of reactions. The higher the absorbance value, the more effective is the complex as a catalyst.

The concept of enzymatic mimetic activities is related to the synthesis of molecules that simulate the active site of an enzyme. Moreover, it is worth noting that this concept is not inflexible. Thus, several articles in the literature have reported reactions similar to those of peroxidase, which use transition metal complexes different from those of natural enzymes (when comparing with data from horseradish peroxidase), such as nickel,<sup>[27,49]</sup> cobalt,<sup>[21]</sup> and copper,<sup>[47]</sup> as well as non-porphyrinic ligands.

However, there are few reports in the literature of mixed-valence complexes with the pro-oxidant activity evaluated in this work. In one of these cases, Horn *et al.* synthesized mixed-valence manganese(III and IV) complexes that were tested as possible peroxidase mimetics; however, the complexes presented more significant results for biomimetics of catalase activity.<sup>[50]</sup>

## 4.2 | Aromatic amine substrate

The readings were conducted at five-minute intervals. A graph was plotted after 2 h to relate the absorbance variation as a function of the time that the samples were irradiated in the spectrophotometer (wavelength of 450 nm). As the oxidation of the initial substrates occurred, absorbance increased, that is, both the formation of TMB diimine and the coupling reaction generated 2,3-diaminophenazine (confirmed by GC-MS analyses; see supporting information).

The isolated ligands do not have mimetic activity because the absorbance values are closer to those obtained in the reaction without a catalyst (blank). In this sense, it is evident that the presence of labile ligands in the coordination sphere of the Co(II) ions is crucial for the activity of the complexes. However, the increase in the organic chain of the organic ligand generated a more positive potential reduction pattern, allowing higher reactivity with hydrogen peroxide. Notably, the three compounds evaluated in this study have similar molecular structures and solvates.

By comparing the data with TMB oxidation, no equilibrium between the radical formation of the charge transfer complex was observed, providing a strong blue coloration despite the diimine generated by the complete oxidation of the TMB substrate (Figure 8). The results found in the literature<sup>[15,30]</sup> illustrate the same total oxidation mechanism, although with different compounds.

Although not presenting zwitterionic characteristics, an expressive example of peroxidase activity reported in the literature was developed by Wang *et al.*,<sup>[51]</sup> who showed that the activation of hydrogen peroxide can also

be achieved by means of nanoparticulate materials, specifically  $\text{Co}_2\text{O}_3$ . By comparing the results to those of this article, similar pro-oxidant activity was observed; however, an advantage of the materials synthesized by Wang *et al.* was the time/activity ratio in which constant increases in the substrate conversion occurred.

Moreover, when the absorbance values for the oxidation of the OPD substrate, which generates 2,3-diaminophenazine (Figure 9), are correlated with those of Guan and co-workers,<sup>[52]</sup> it is possible to observe that the zwitterionic complex containing a four-carbon-atom chain (ZW4C) also presented the best oxidation results (confirmed by GC-MS analyses; see supporting information).

All complexes exhibit Co(III)/Co(II) reduction and Co(II)/Co(III) re-oxidation processes, that is, each complex reduces, although it is regenerated after electrochemical oxidation. The redox potential values for the cobalt complexes in this study were observed between  $-0.18$  and  $-0.55$  V versus NHE. When compared with the values found for the reduction of the native enzyme horseradish peroxidase ( $E = -0.306$  V versus NHE) in the literature, the zwitterionic cobalt complexes have reduction processes similar to the native enzyme (only in terms of oxidation potential, as the activity itself is still lower). This indicates that they may present activity similar to that of the peroxidase of this plant (horseradish).<sup>[53]</sup>

Activation of hydrogen peroxide catalyzed by cobalt complexes is often associated with the formation of reactive oxygen species such as superoxide radicals, hydroxyl, and hydroperoxide.<sup>[54–57]</sup> These species are versatile oxidants for various organic substrates; however, due to their radical nature and consequently high reactivity, they

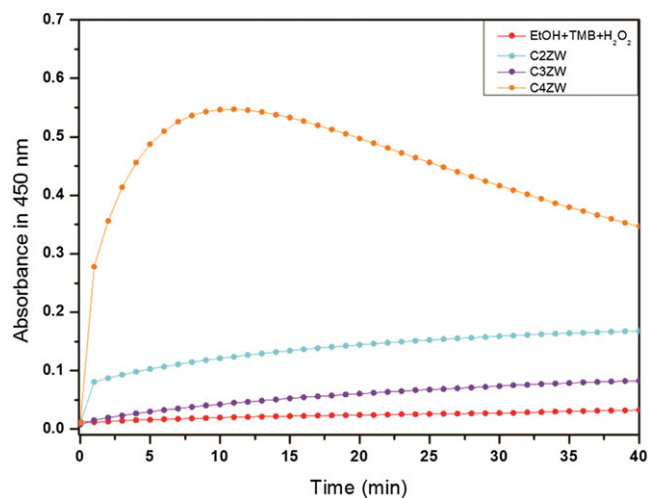


**FIGURE 8** Absorbance plot (450 nm) in relation to time of mixed-valence Co complexes

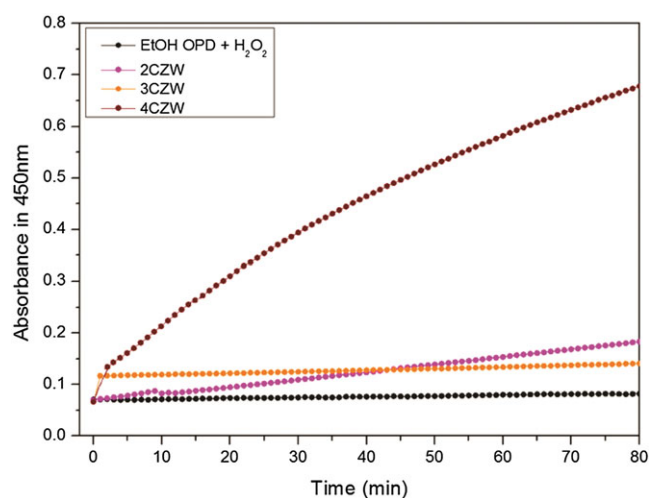


**FIGURE 9** Absorbance plot (450 nm) in relation to time of Co complexes with mixed valence

must be generated in the reaction medium itself. The cobalt dinuclear complexes developed in this work have different coordination environments and oxidation states, one of which is octahedral Co(III) and the other tetrahedral Co(II). In these complexes, the Co(II) atom is less protected by the ligands when compared to the Co(III) atom, and therefore it must be the main reactive site (which is also corroborated by density functional theory calculations), effectively interacting with hydrogen peroxide and promoting its activation. Thus, by assuming that the Co(II) site is catalytic, it is plausible to believe that the same reactional behavior described by Lázaro-Martínez<sup>[54]</sup> and Liang<sup>[55]</sup> can occur in the three complexes investigated in this work.

## 5 | CONCLUSIONS

Due to the coordination formed by a ligand containing oxygen, nitrogen, and sulfur atoms, based on pro-oxidant activity observed in experiments, we believe that peripheral Co(II) moiety may be related to peroxidase activity. However, the three complexes present similar coordination spheres, thus little difference was observed in stereochemical reactivity. The main difference was revealed by the cyclic voltammetry analysis of the complexes, in which the complex ZW4C exhibited more pronounced changes in regions of higher positive potential, thus indicating the possible existence of (*in situ*) Co<sup>III</sup> ions.<sup>[58,59]</sup>

Therefore, we attribute the best peroxide activation behavior to the complex with more reversible redox processes, such as the zwitterionic complex containing a sulfur-ligand butyl substituent. Along with these observations, density functional theory calculations showed that there is corroboration between metallic atoms, that is, a higher nucleophilic activity in the two metallic centers, a situation which was not evidenced in the other two complexes. Reports of pro-oxidant activities of zwitterionic complexes are scarce; therefore, the results of this work are innovative.

## ACKNOWLEDGEMENTS

We thank the financial agencies: Brazilian Research Councils: CNPq – Edital no. 14/2014/Proc. Num. 444780/2014-9, Edital no. 12/2016/Proc. Num. 303011/2016-5 and Edital no. 28/2018/Proc. Num. 424514/2018-4; UFSM/CNPQ-PIBIC-2016 (043272); CNPq – Edital no. 443625-2014-0; FAPERGS (Edital 02/2017 – PqG).

## SUPPLEMENTARY DATA

CCDC 1833006, 1833011, 1833139, and 1835012 contain the supplementary crystallographic data for complexes ZW2C, ZW3C and ZW4C and ligand L2C (supporting information), respectively. These data can be obtained free of charge via <http://www.ccdc.cam.ac.uk/conts/retrieving.html>, or from the Cambridge Crystallographic Data Centre, 12 Union Road, Cambridge CB2 1EZ, UK; fax: (+44) 1223 336 033; or e-mail: [deposit@ccdc.cam.ac.uk](mailto:deposit@ccdc.cam.ac.uk).

## ORCID

Bernardo Almeida Iglesias  <https://orcid.org/0000-0002-4039-6316>

Davi Fernando Back  <https://orcid.org/0000-0002-9107-1503>

## REFERENCES

- [1] C. Celik, M. Tumer, S. Serin, *Synth. React. Inorg. Met. Org. Nano-Met. Chem.* **2002**, *32*, 1839.
- [2] L. Lekha, K. K. Raja, G. Rajagopal, D. Easwaramoorthy, *J. Organometal. Chem.* **2014**, *753*, 72.
- [3] N. Karabocek, S. Karabocek, F. Kormali, *Turk. J. Chem.* **2007**, *31*, 271.
- [4] D. Desbouis, I. P. Troitsky, M. J. Belousoff, L. Spiccia, B. Graham, *Coord. Chem. Rev.* **2012**, *256*, 897.
- [5] B. Kupcewicz, K. Sobiesiak, K. Malinowska, K. Koprowska, M. Czyz, B. Keppler, E. Budzisz, *Med. Chem. Res.* **2013**, *22*, 2395.
- [6] Y. Noritake, N. Umezawa, N. Kato, T. Higuchi, *Inorg. Chem.* **2013**, *52*, 3653.
- [7] K. M. Light, Y. Yamanaka, M. Odaka, E. I. Solomon, *Chem. Sci.* **2015**, *6*, 6280.
- [8] S. Miriyala, I. Spasojevic, A. Tovmasyan, D. Salvemini, Z. Vujaskovic, D. St. Clair, I. Batinic-Haberle, *Biochim. Biophys. Acta* **2012**, *1822*, 794.
- [9] B. V. Plapp, B. R. Savarimuthu, D. J. Ferraro, J. K. Rubach, E. N. Brown, S. Ramaswamy, *Biochemistry* **2017**, *56*, 3632.
- [10] S. Sarkar, K. Dey, *Spectrochim. Acta A* **2005**, *62*, 383.
- [11] J. S. Casas, D. Couce, J. Sordo, *Coord. Chem. Rev.* **2012**, *256*, 3036.
- [12] S. Sharif, D. Schagen, M. D. Toney, H. H. Limbach, *J. Am. Chem. Soc.* **2007**, *129*, 4440.
- [13] E. C. Niederhoffer, J. H. Timmons, A. E. Martel, *Chem. Rev.* **1984**, *84*, 137.
- [14] C. Bianchini, R. W. Zoellner, *Adv. Inorg. Chem.* **1997**, *44*, 263.
- [15] N. Li, Y. Yan, B.-Y. Xia, J.-Y. Wang, X. Wang, *Biosens. Bioelectron.* **2014**, *54*, 521.
- [16] S. Çai, Q. Han, C. Qi, Z. Lian, X. Jia, R. Yang, C. Wang, *Nanoscale* **2016**, *8*, 3685.
- [17] H. Jiang, Z. Chen, H. Cao, Y. Huang, *Analyst* **2012**, *137*, 5560.

- [18] F. Van de Velde, F. van Rantwijk, R. A. Sheldon, *Trends Biotechnol.* **2001**, *19*, 73.
- [19] C. Ray, S. Dutta, S. Sarkar, R. Sahoo, A. Roy, T. Pal, *J. Mater. Chem. B* **2014**, *2*, 6097.
- [20] A. Córdoba, N. Alasino, M. Asteasuain, I. Magario, M. L. Ferreira, *Chem. Eng. Sci.* **2015**, *129*, 249.
- [21] Q. Liu, Y. Yang, H. Li, R. Zhu, Q. Shao, S. Yang, J. Xu, *Biosens. Bioelectron.* **2015**, *64*, 147.
- [22] R. R. Gagne, C. A. Koval, G. C. Lisensky, *Inorg. Chem.* **1980**, *19*, 2854.
- [23] G. M. Sheldrick, *Acta Crystallogr.* **2008**, *A64*, 112.
- [24] K. Brandenburg, DIAMOND 3.1a, 1997–2005, Version 1.1a. Crystal Impact GbR, Bonn, Germany.
- [25] D. Li, Y. Tong, J. Huang, L. Ding, Y. Zhong, D. Zeng, P. Yan, *J. Mol. Catal. A* **2011**, *345*, 108.
- [26] Y. Li, H. Zhang, F. Cao, *J. Sol-Gel Sci. Technol.* **2011**, *58*, 156.
- [27] L. A. Fontana, M. Stüker, G. M. Oliveira, B. A. Iglesias, D. F. Back, *Inorg. Chem. Commun.* **2015**, *62*, 55.
- [28] M. Li, X.-R. Huang, Y. Guo, Y.-Z. Shang, H.-L. Liu, *Chin. Chem. Lett.* **2017**, *28*, 1453.
- [29] M. Chen, L. Sun, Y. Ding, Z. Shi, Q. Liu, *New J. Chem.* **2017**, *41*, 5853.
- [30] L. Guo, S. Xu, X. Ma, B. Qiu, Z. Lin, G. Chen, *Sci. Rep.* **2016**, *6*, 32755.
- [31] N. S. Surgutskaya, M. E. Trusova, G. B. Slepchenko, A. S. Minin, A. G. Pershina, M. A. Uimin, A. E. Yermakov, P. S. Postnikov, *Anal. Methods* **2017**, *9*, 2433.
- [32] H. Wang, W. Jiang, Y. Wang, X. Liu, J. Yao, L. Yuan, Z. Wu, D. Li, B. Song, H. Chen, *Langmuir* **2013**, *29*, 3.
- [33] W. J. Stevens, M. Krauss, H. Basch, P. G. Jasien, *Can. J. Chem.* **1992**, *70*, 612.
- [34] M. J. Frisch, G. W. Trucks, H. B. Schlegel, G. E. Scuseria, M. A. Robb, J. R. Cheeseman, G. Scalmani, V. Barone, G. A. Petersson, H. Nakatsuji, X. Li, M. Caricato, A. Marenich, J. Bloino, B. G. Janesko, R. Gomperts, B. Mennucci, H. P. Hratchian, J. V. Ortiz, A. F. Izmaylov, J. L. Sonnenberg, D. Williams-Young, F. Ding, F. Lipparini, F. Egidi, J. Goings, B. Peng, A. Petrone, T. Henderson, D. Ranasinghe, V. G. Zakrzewski, J. Gao, N. Rega, G. Zheng, W. Liang, M. Hada, M. Ehara, K. Toyota, R. Fukuda, J. Hasegawa, M. Ishida, T. Nakajima, Y. Honda, O. Kitao, H. Nakai, T. Vreven, K. Throssell, J. A. Montgomery Jr., J. E. Peralta, F. Ogliaro, M. Bearpark, J. J. Heyd, E. Brothers, K. N. Kudin, V. N. Staroverov, T. Keith, R. Kobayashi, J. Normand, K. Raghavachari, A. Rendell, J. C. Burant, S. S. Iyengar, J. Tomasi, M. Cossi, J. M. Millam, M. Klene, C. Adamo, R. Cammi, J. W. Ochterski, R. L. Martin, K. Morokuma, O. Farkas, J. B. Foresman, D. J. Fox, Gaussian 09, Revision C. Gaussian Inc., Wallingford, CT, **2016**.
- [35] G. A. Zhurko, Chemcraft: graphical program for visualization of quantum chemistry computations, <http://www.chemcraftprog.com>
- [36] T. Steiner, *Angew. Chem. Int.* **2002**, *41*, 48.
- [37] G. A. Jeffrey, *An Introduction to Hydrogen Bonding*, Oxford University Press, Oxford **1997**.
- [38] P. Pattanayak, J. L. Pratihar, D. Patra, C. H. Lin, S. Paul, K. Chakraborty, *Polyhedron* **2013**, *51*, 275.
- [39] P. Pattanayak, J. L. Pratihar, D. Patra, C. H. Lin, P. Brandão, D. Mal, V. Felix, *J. Coord. Chem.* **2013**, *66*, 568.
- [40] S. Anbu, S. Kamalraj, B. Varghese, J. Muthumary, M. Kandaswamy, *Inorg. Chem.* **2012**, *51*, 5580.
- [41] R. Fekri, B. Shaabani, *J. Appl. Environ. Biol. Sci.* **2013**, *3*, 75.
- [42] R. Shakya, C. Imbert, H. P. Hratchian, M. Lanznaster, M. J. Heeg, B. R. McGarvey, M. Allard, H. B. Schlegel, C. N. Verani, *Dalton Trans.* **2006**, *21*, 2517.
- [43] P. Pattanayak, J. L. Pratihar, D. Patra, P. Brandão, V. Felix, *Inorg. Chim. Acta* **2014**, *418*, 171.
- [44] M. Aslantas, E. Kendi, N. Demir, A. E. Sabıkc, M. Tmer, M. Kertmend, *Spectrochim. Acta A* **2009**, *74*, 617.
- [45] A. H. Kianfar, M. Sedighipoor, G. Mohammadnezhad, H. Grls, W. Plass, M. Roushani, *J. Iranian Chem. Soc.* **2017**, *14*, 313.
- [46] W. Zhu, S. Zhang, C. Cui, F. Bi, H. Ke, G. Xie, S. Chen, *Inorg. Chem. Commun.* **2014**, *46*, 315.
- [47] H. Y. Kim, H. J. Lee, S. K. Chang, *Talanta* **2015**, *132*, 625.
- [48] Y. Xiong, S. Chen, F. Ye, L. Su, C. Zhang, S. Shen, S. Zhao, *Anal. Methods* **2015**, *7*, 1300.
- [49] V. G. Organo, A. S. Filatov, J. S. Quartararo, Z. M. Friedman, E. V. RybakAkimova, *Inorg. Chem.* **2009**, *48*, 8456.
- [50] J. A. Lessa, A. Horn Jr., E. S. Bull, M. R. Rocha, M. Benassi, R. R. Catharino, M. N. Eberlin, A. Casellato, C. J. Noble, G. R. Hanson, G. Schenk, G. C. Silva, O. A. C. Antunes, C. Fernandes, *Inorg. Chem.* **2009**, *48*, 4569.
- [51] J. Mu, Y. Wang, M. Zhao, L. Zhanga, *Chem. Commun.* **2012**, *48*, 2540.
- [52] J. Guan, J. Peng, X. Jin, *Anal. Methods* **2015**, *7*, 5454.
- [53] G. Battistuzzi, M. Borsari, A. Ranieri, M. Sola, *J. Am. Chem. Soc.* **2002**, *124*, 26.
- [54] J. M. Lázaro-Martínez, L. V. L. Lupano, L. L. Piehl, E. RodríguezCastellon, V. C. Dall' Orto, *J. Phys. Chem. C* **2016**, *120*(51), 29332.
- [55] S. Liang, L. Zhao, B. Zhang, J. Lin, *Chem. Eur. J.* **2008**, *112*, 618.
- [56] C. Shen, S. Song, L. Zang, X. Kang, Y. Wen, W. Liu, L. Fu, *J. Hazard. Mater.* **2010**, *177*, 560.
- [57] B. Agboola, K. I. Ozoemena, T. Nyokong, *J. Mol. Catal. A* **2005**, *227*, 209.
- [58] D. H. Kim, U. S. Shin, C. E. Song, *J. Mol. Catal. A* **2007**, *271*, 70.
- [59] M. Hatazawa, K. Nakabayashi, S. I. Ohkoshi, K. Nozaki, *Chem. Eur. J.* **2016**, *22*, 13677.
- [60] G. Rajsekhar, C. P. Rao, P. K. Saarenketo, E. Kolehmainen, K. Rissanen, *Inorg. Chem. Commun.* **2002**, *5*, 649.
- [61] N. Roy, S. Sproules, E. Bothe, T. Weyhermiller, K. Wieghard, *Eur. J. Inorg. Chem.* **2009**, 2655.
- [62] J. C. Noveron, M. M. Olmstead, P. K. Mascharak, *J. Am. Chem. Soc.* **1999**, *121*, 3553.
- [63] S. Pal, P. Sengupta, S. Ghosh, G. Mukherjee, G. Mostafa, *J. Coord. Chem.* **2002**, *55*, 271.
- [64] X. Zou, J. Zhang, L. Zhang, Y. Liu, N. Li, Y. Li, S. Wei, M. Pan, *Inorg. Chem. Commun.* **2015**, *54*, 21.
- [65] L. Stefan, F. Denat, D. Monchard, *Nucleic Acids Res.* **2012**, *40*, 8759.
- [66] P. GeottiBianchini, T. Darbre, J.L. Reymond, *Org. Biomol. Chem.* **2013**, *11*, 344.

- [67] A. Long, P. Rothenberg, D. Patel, J. MacDougall, M. R. Hartings, *Polyhedron* **2016**, *114*, 138.

### SUPPORTING INFORMATION

Additional supporting information may be found online in the Supporting Information section at the end of the article.

**How to cite this article:** Fontana LA, Siqueira JD, Ceolin J, et al. Peroxidase activity of new mixed-valence cobalt complexes with ligands derived from pyridoxal. *Appl Organometal Chem.* 2019;e4903. <https://doi.org/10.1002/aoc.4903>